Highly charged ions impinging on a stepped metal surface under grazing incidence

A. Robin,[1,2] D. Niemann,[3] N. Stolterfoht,[3] and W. Heiland[2]
[1]*KVI Atomic Physics, Rijksuniversiteit Groningen, Zernikelaan 25, NL-9747 AA Groningen, The Netherlands*
[2]*Universität Osnabrück, D-49069 Osnabrück, Germany*
[3]*Hahn-Meitner-Institut Berlin, Glienicker Strasse 100, D-14109 Berlin, Germany*
(Received 1 November 2002; published 13 May 2003)

We report on energy loss measurements and charge state distributions for 60 keV N^{6+} and 75 keV N^{5+} ions scattered off a Pt(110)(1×2) single crystal surface. In particular, the influence of surface steps on the energy loss and the outgoing charge states is discussed. The scattering angle and the angle of incidence are varied. We use grazing incidence conditions, i.e., the momentum perpendicular to the surface is low enough to prevent penetration through the first atomic layer. Image charge effects are observed leading to an additional projectile acceleration towards the surface. Outgoing charge states are detected from $1+$ up to $3+$. Axial channeling conditions are defined by scattering along the azimuthal [001] direction, i.e., the projectiles are guided along the [001]-atomic rows. The energy loss for axial channeling is found to be somewhat larger and the energy distribution to be broadened in comparison with the spectra for planar channeling conditions. The broadening is attributed to the interaction of the projectiles with the side wall potentials of the surface channels. We find a strong increase in the energy loss with increasing scattering angle, which exceeds the calculated contribution of the elastic energy transfer by orders of magnitudes. These increased energy losses are attributed to the interaction of the ions with the surface steps.

DOI: 10.1103/PhysRevA.67.052901 PACS number(s): 34.50.Bw, 34.50.Dy, 61.85.+p, 79.20.Rf

I. INTRODUCTION

Highly charged ions (HCIs) interacting with surfaces lead to very interesting phenomena. Because of the high potential energy involved, a cascade of processes takes place, leading, e.g., to electron and plasmon excitations [1], x-ray, electron, and particle emission (see, e.g., [2–6]). Many experimental methods such as x-ray photoemission spectroscopy, Auger-electron spectroscopy, secondary electron emission, etc., have been used to investigate these phenomena, shedding light on the neutralization processes of HCIs and the respective time scales [7–12]. Investigations of the scattered projectiles give insight into image charge acceleration effects [13] and, in combination with computer simulations, yield information about trajectory dependencies of the energy loss and charge state distributions [14–16]. Out-of-plane scattering events, or zig-zag scattering, may strongly influence the energy loss of the projectiles [17]. At grazing incidence the *zig-zag* events cause an additional broadening of the angular and energy distributions of the scattered particles [8,18].

This paper investigates the influence of surface steps on the energy loss and charge state distributions of the scattered ions. We report on measurements with primary 60 keV N^{6+} and 75 keV N^{5+} ions scattered off a Pt(110)(1×2) single crystal surface, i.e., the projectile velocity v stays below $0.5v_0$ with v_0 the Bohr velocity. Neutrals cannot be detected with the applied experimental method, but previous surface scattering studies have shown that the neutral fraction of scattered projectiles is at least 85% for the presented ions and energies [8]. Estimations of the mean charge states for the presented projectile-surface combination and ion energies result in values between 0.5 and 0.8. However, these estimations are restricted to fast ($v\gtrsim v_0$) and heavy ($Z\geqslant16$) ions [19] and do not include surface contributions to the neutralization process.

II. EXPERIMENTAL ASPECTS

The experiments were carried out at the Ionenstrahl-Labor in Berlin. The beam was produced in the 14.5-GHz electron cyclotron resonance source and collimated to a diameter of about 1 mm. The absolute energy uncertainty is estimated to be on the order of 2%, whereas the energy broadening is estimated to be less than ~15 eV$\times q$ with q the primary charge state. Primary beams of 60 keV N^{6+} and 75 keV N^{5+} are directed towards the cleaned crystal surface under the grazing angle of incidence ψ varying from 0.5° up to 10°. Crystal preparation is done in an ultrahigh vacuum chamber [10] with a base pressure in the low 10^{-9} mbar range by successive Ar^+ sputtering and annealing. Using the target preparation recipe known from previous scanning tunnel microscope (STM) studies [20], the clean Pt(110) crystal forms the (1×2) missing row structure. Every other $[1\bar{1}0]$ chain is missing resulting in wide surface semichannels. The surface reconstruction is controlled by low-energy electron diffraction. Mesoscopically, a fish scale pattern (rhomboidal shape) is formed with elongated terraces of 50–60 nm length and 15–30 nm width, i.e., along the [001] direction the average step length L_S for a consecutive upward and downward step is in the range of the average trajectory length L_T. The azimuthal angle ϕ is varied between the axial channeling conditions along the [001] direction ($\phi=90°$) and the surface planar channeling ($\phi=80°$). The scattering geometry is shown in the inset of Fig. 1.

We use an electrostatic analyzer with a special deflection plate geometry, making it possible to measure high energy particles with low deflection voltages [21,22]. Neutrals cannot be detected. The detector acceptance angle for surface scattered particles depends on the scattering angle. For θ between 1° and 20° the acceptance angle varies between 0.5° and 2°, having a small effect on the measured spectral

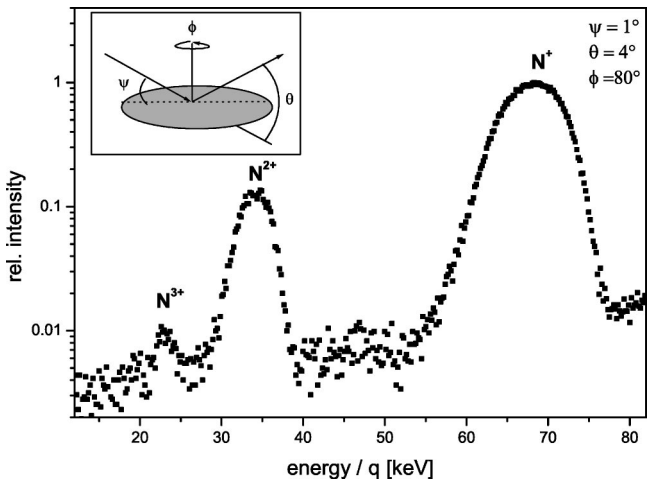

FIG. 1. Scattering of 75 keV N^{5+} off a Pt(110)(1×2) surface. The raw spectra shows three different contributions, which we attribute to scattered N^+, N^{2+}, and N^{3+} ions, respectively. The inset shows the scattering geometry.

broadening. We obtain a total energy resolution of approximately 2% including angular straggling. The energy calibration of the analyzing system is exact to within 1% [21]. Together with the primary energy uncertainty, we can measure the energy of the scattered particles to within an accuracy of 3%. In summary, our detection system allows the measurement of energy spectra for different scattered charge states, whereas absolute quantitative energy losses are hardly available. Nevertheless, rough features and relative changes in the spectra for different scattering parameters ϕ, ψ, and θ are well reproduced.

III. RESULTS AND DISCUSSION

A typical raw spectrum is given in Fig. 1 for 75 keV N^{5+} showing three different distributions, which we attribute to scattered N^+, N^{2+}, and N^{3+}. There are some indications for N^{4+} in the energy spectra in the case of $\phi=80°$, but due to the weak signal-to-noise ratio a quantitative analysis is not possible. In contrast, the 60 keV N^{6+} spectra show no indication of any higher outgoing charge states than N^{2+}.

After subtracting a background function we analyze the different peaks concerning scattering intensity, mean energy, and energy broadening. The Gaussian fits to the different peaks in the measured spectra give us mean energy values $\overline{E}$ for the respective charge states. From them we calculate the mean energy loss ΔE defined as the difference between the primary energy E_0 and $\overline{E}$. The results from this procedure will be discussed in Sec. III B. By calculating the peak area with regard to different scattered charge states, we obtain the scattering intensity for the respective scattering geometry. This procedure is done for all scattering angles resulting in scattering intensity distribution as shown in Fig. 2. In a following step, we will investigate the intensity ratios $I(N^{2+})/I(N^+)$ and $I(N^{3+})/I(N^+)$ to gain information about the neutralization process, as discussed in Sec. III C.

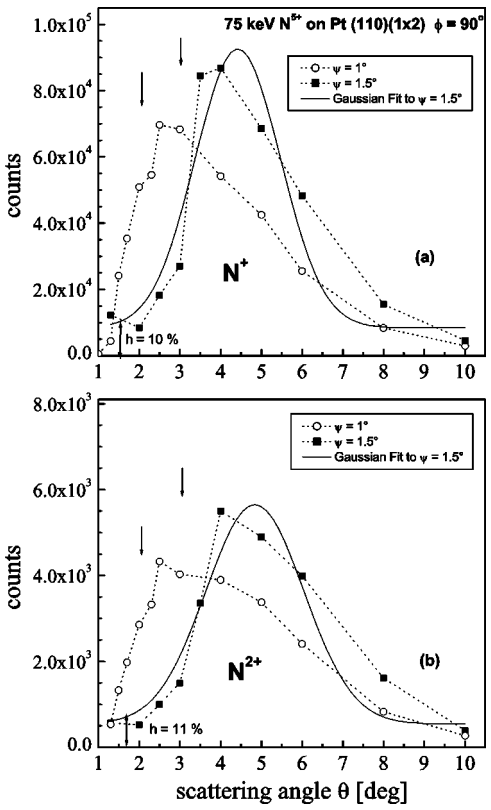

FIG. 2. N^+ intensity vs scattering angle in case of 75 keV N^{5+} scattering along the [001] surface direction under the incident angles of $\psi=1°$ and $\psi=1.5°$, respectively (a). Additionally, for $\psi=1.5°$, a Gaussian fit is shown (solid line). Arrows mark the angle of specular reflection. The step-density parameter h measures the percentage of the foot intensity compared to the maximum intensity. (b) Same as (a) for the scattered N^{2+} intensity.

A. Scattering intensity

Since the highly charged ions are attracted on the incoming path by the image force, this results in an energy gain of 15 eV for 75 keV N^{5+} and 23 eV for 60 keV N^{6+}. The values are calculated from the staircase model of stepwise neutralization [23], resulting in an acceleration of the ions towards the surface. As a result one observes a shift of the maximum in the scattering distribution towards higher scattering angles. Experimental results for flat crystalline surfaces are in very good agreement with the model predictions [13,21,22,24,25]. A necessary condition in order to determine quantitatively the image interaction by the above discussed technique is excellent control of the surface quality and roughness. The use of a stepped surface may change the scattering conditions significantly. In our measurements we observe shifts of the peak maxima (Fig. 2), which exceed by $\sim 0.7°$ for $\psi=1°$ and by $\sim 0.8°$ for $\psi=1.5°$ the calculated values. The calculations are based on specular reflection scattering and include image force effects. This effect has been found in earlier studies as well [9,22], indicating surface imperfections.

We observe a broadening of the experimental scattering distribution, which is approximately 30% larger than that calculated from the MARLOWE code [22] and increases with a

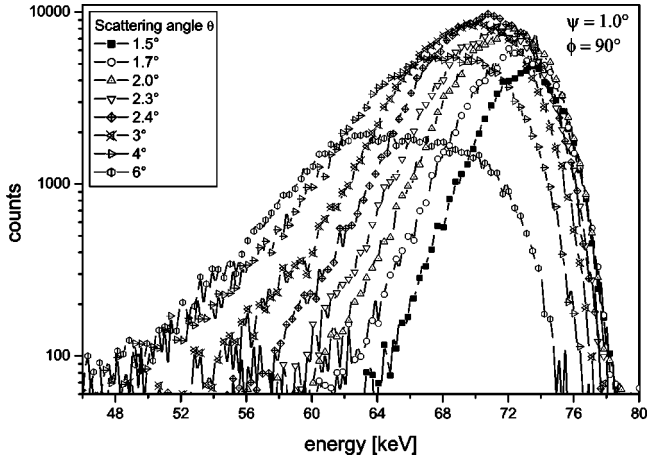

FIG. 3. Energy spectra series for scattered N^+ with variation of the scattering angle θ. The angle of incidence is fixed at $\psi=1°$, the scattering plane is along the [001]-surface direction ($\phi=90°$).

decreasing angle of incidence and an increasing outgoing charge state. Both phenomena might be taken as indicators for surface step collisions. Additionally, we find an asymmetry in the scattering distribution towards higher scattering angles (Fig. 2), which indicates collisions with upward steps [24]. Therefore, a high surface step density is assumed. Pfandzelter has simulated scattering distributions for H ions interacting with stepped Al surfaces [24], where he found an average step length L_S of $\sim$300 Å for a value of 10–11 % of the step density parameter h (Fig. 2). The h value measures the intensity ratio between the peak maximum and the low-scattering-angle foot, which is caused by collisions with downward steps. This result is in good agreement with the STM measurements from Speller *et al.* [20], claiming an average step length along the [001] direction of $L_S = 150$–300 Å.

B. Energy spectra

From the scattering intensity distribution we know already that projectile-step interactions take place during the scattering process. It is now interesting to look at how the step scattering influences the energy spectra. Figure 3 shows a series of energy spectra for scattered N^+ ions with varying θ. The count rate is plotted against the energy. We observe a clear shift of the peak maximum to lower energies with increasing scattering angle, i.e., the outgoing path has a strong influence on the energy loss of the scattered particles. Taking the mean energy values from a Gaussian fit to the energy maxima of the respective charge states, we find that the energy loss ΔE increases mostly linear up to a scattering angle of 6°–8° (Fig. 4). This observation holds for all detected charge states [Fig. 4(b)]. For $\theta>8°$, ΔE seems to saturate. A closer look shows an additional feature around $\theta\simeq 2\psi$, where the energy loss increase with θ seems to be slightly lowered. At the same time the spectral width increases more strongly than expected from a linear dependency on θ. These effects indicate surface channeling, i.e., they are not present for larger angles of incidence, as will be seen in Sec. III D. Basically, the energy broadening given in the inset of Fig.

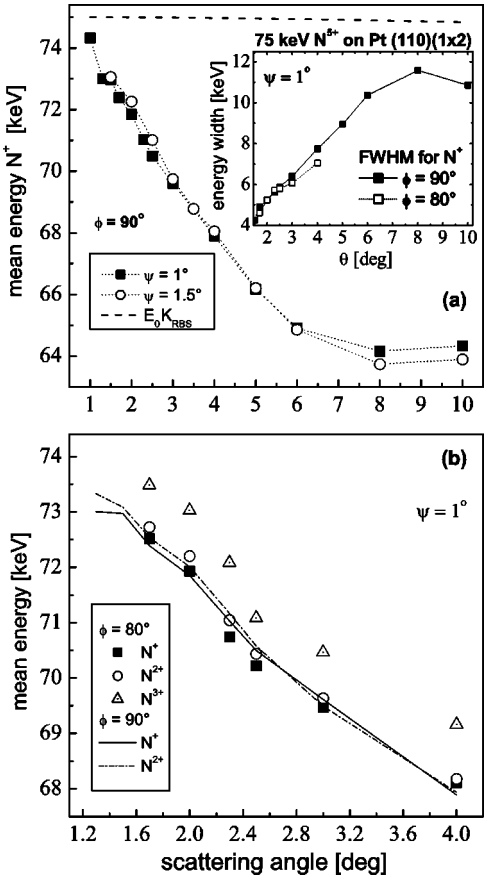

FIG. 4. Mean energy values obtained from the Gaussian fits to the energy spectra shown, e.g., in Fig. 3. (a) compares the results for $\psi=1°$ and $\psi=1.5°$. The dashed line gives the calculated elastic energy transfer for a single binary collision. Inset shows the energy broadening plotted as the full width of half maximum for both the azimuthal directions. (b) shows the mean energy values for different outgoing charge states for axial and planar channeling. Lines are drawn to guide the eye.

4(a) shows a similar dependency on θ as the energy loss does. The θ dependency of the detector acceptance angle contributes only $\sim$10–15 % to the observed increase of the energy broadening for the small θ variations under consideration. The clear increase of the spectral broadening with θ is, therefore, to a great extent, caused by nonspecular and nonplanar scattering events. In fact, extended trajectory straggling leads to a broadened energy spectrum, as is confirmed by the stronger spectral broadening due to axial channeling in the case of $\phi=90°$ compared to the planar channeling case at $\phi=80°$. The additional broadening in the case of axial channeling is due to interactions with the side walls of the surface channels leading to elongated zig-zag trajectories, which are also found in trajectory calculations [17]. Zig-zag scattered particles undergo more scattering processes than particles scattered along a random direction, leading to enhanced energy losses, and to a broadened straggling tail in the spectra. However, the effect seen for the [001] direction is not as strong as that observed for scattering along the $[1\bar{1}0]$ direction [15,17].

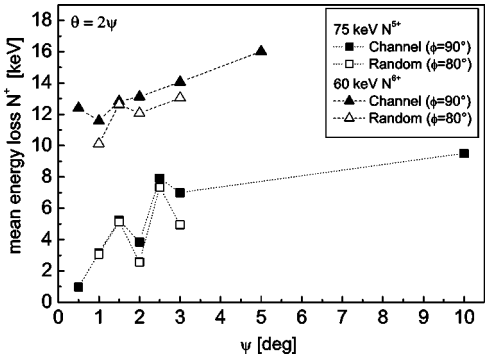

FIG. 5. Mean energy loss dependency on ψ for specular-reflection scattering. Lines are drawn to guide the eye.

The results concerning the θ behavior do not strongly depend on the angle of incidence, which is an indication that the distribution of outgoing particle trajectories is mostly unaffected by the incoming geometry. However, particles following steeper incoming trajectories, i.e., having larger incidence angles, show enhanced energy losses (Fig. 5). Though the dependency on ψ is not as straightforward as on θ, we find an increase for N^{5+} of ΔE up to $\psi=1.5°$ ($E_{\perp} \approx 52$ eV) and a kind of saturation for $\psi \geqslant 2.5°$ attributed to the transition from surface to bulk scattering [14]. The energy loss behavior on ψ and the increased energy losses found for incoming N^{6+} are not completely understood yet, since the deviations are clearly outside the error bars of the system ($\Delta E^{error} \sim 2$–3 keV). The effect for N^{6+} may be caused by enhanced charge exchange and excitation processes during the neutralization on the incoming trajectory path. Nevertheless, we cannot rule out that the uncertainty in the determination of the primary energy is larger than assumed.

Looking at Fig. 4(b) we find the same energy loss dependency on θ for different scattered charge states and both azimuths ϕ. On average, the energy loss of scattered N^{2+} is found to be $\sim$200–300 eV less and that of scattered N^{3+} to be ~ 1 keV less than the loss of scattered N^{+}. This tendency was found earlier [14,26], but is in contrast to transmission experiments. In principle, the amount of processes contributing to the inelastic energy loss is found to increase with higher charge states when charged particles interact with an electron gas [27]. Hence, it can be assumed that different higher charge states follow different trajectories originating, e.g., from scattering processes off downward steps, which suddenly interrupt the interaction with the surface leading to lower energy losses. Consequently, we expect that different electron densities are probed by different charge states, leading to different energy losses. We conclude that a separation of the outgoing charge states permits selection of different trajectory ensembles.

C. Neutralization process

Taking the former findings into account, we conclude that the kind of scattering process and the outgoing conditions determine the scattered charge state, not the incoming conditions. Consequently, the neutralization process must have been completed already on the incoming particle trajectory, i.e., at relatively large surface distances and within a short-time scale of approximately 10 fs. This assumption is supported by other experiments analyzing outgoing ions [13] and emitted electrons [28]. Furthermore, our results concerning the scattered charge state ratios presented in Fig. 6 support this finding. Despite the greater probability of complete neutralization due to the increased interaction time in the case of $\psi=1°$ compared to the case of $\psi=1.5°$, we obtain a slightly larger charge state ratio $I(N^{2+})/I(N^{+})$ in the case of $\psi=1°$.

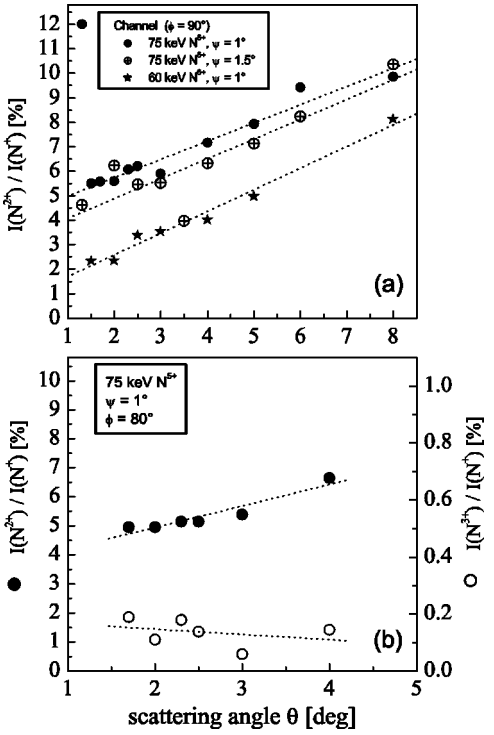

FIG. 6. Experimental charge state ratios $I(N^{2+})/I(N^{+})$ (left scale) and $I(N^{3+})/I(N^{+})$ (right scale) depending on the scattering angle θ for different primary ions. (a) uses axial scattering conditions, (b) is for $\phi=80°$. Dotted lines are linear fits to the experimental data.

Additionally, Fig. 6 shows that the intensity ratio $I(N^{2+})/I(N^{+})$ is lower for incoming N^{6+} (2–8 %) than for primary N^{5+} ions (4–10 %) for all scattering angles under consideration. This indicates a loss of memory of the initial *K*-shell hole of N^{6+}, which does not survive the incoming trajectory. In the case of N^{6+} we would otherwise measure a pronounced production of higher outgoing charge states [26,29]. The fast neutralization of the nitrogen ions might be supported by a relatively high electron density of platinum with a free-electron radius of $r_s=1.63$ a.u. for the bulk. Besides this, the exchange probability between a nitrogen *K*-shell hole and a platinum N_{1-3} subshell was calculated depending on the internuclear distance by Schippers [28]. It turned out that the exchange probability is between 74% and 100% for different Pt subshells N_{1-3} at the respective crossing points of the Pt-N potential curves. These crossing points are located at internuclear distances between 0.6 and 1 a.u. Looking at higher outgoing charge states, we find a percent-

age of N^{3+} which is ~25 times lower than the percentage of N^{2+} and does not significantly depend on θ. This may indicate that the creation process for N^{3+} is different from that for N^{2+}, e.g., the production rate of scattered N^{3+} ions may be mainly related to the particle velocity. Since we do not have evidence for scattered charge states higher than N^{2+} in the case of the slower 60 keV N^{6+} primary ions, this assumption seems reasonable.

In conclusion, we can separate the scattering into the following steps. After neutralization on the incoming path, the projectiles interact strongly with the surface steps, where charge exchange and excitation processes lead to reionization and intensified energy losses of the projectile. The outgoing charge state is, to a great extent, determined by the surface step collisions, which suddenly switch the interaction on or off. The lower electron density outside the surface steps prevents a complete reneutralization of the ions. This model is similar to the freezing-distance model proposed by Mannami *et al.* [30], which has been applied to projectiles with higher velocities scattered off flat surfaces, where charge exchange only takes place in a region of 2 Å near the surface. In our case, the N^{2+} percentage depends on the step density, which is smaller for $\phi=80°$ than along the [001]-surface direction [20]. This results in a slightly higher N^{2+}-to-N^{+} charge ratio for $\phi=90°$ of ~0.5–1 % (Fig. 6). The same effect holds for a variation of ψ. With decreasing ψ the trajectory length L_T increases. As a consequence, the probability of hitting a surface step rises and causes the higher charge state ratio $I(N^{2+})/I(N^{+})$ in the case of $\psi=1°$ compared to $\psi=1.5°$ [Fig. 6(a)].

The above arguments are supported by the higher mean scattering angle for scattered N^{2+} compared to N^{+} (Fig. 2), which was found earlier by Meyer *et al.* [9]. Since step collisions interrupt the planar surface potential, step-scattering processes can cause larger scattering angles when scattering at upward steps. Additionally, surface step collisions lead to an enhanced ionization rate, explaining the increase of the ratio $I(N^{2+})/I(N^{+})$ with increasing scattering angle. However, the monotonic increase of the mean energy loss with θ is not yet clear from these simple assumptions (Fig. 4).

D. Step scattering

How can we explain the strong dependency of the energy loss ΔE on θ? Theoretical energy loss calculations assume planar channeling conditions (see Ref. [15] for details). As input we evaluate the trajectory length L_T from a Monte Carlo code developed by Schippers *et al.* [8], using the Ziegler-Biersack-Littmark (ZBL) scattering potential [31]. We obtain trajectory lengths between 160 and 250 Å for $\phi=80°$ and between 180 and 430 Å for $\phi=90°$, which strongly depend on θ. Hereby, the image force reduces the trajectory length L_T by ~10%. Different trajectory classes are found in the case of axial channeling originating from scattering off the first and the second atomic layer, respectively.

From the relation $\Delta E=S_e L_T$ with $S_e=1.44v$ [a.u.] corresponding to ~20 eV/Å as theoretical electronic stopping power, which is calculated by using the transport cross section at the Fermi level for the electrons scattered at the projectile potential [15,32], we obtain theoretical energy loss values of ΔE^{theo}~3–4.6 keV for $\phi=80°$ and ΔE^{theo} ~3.2–7.8 keV for $\phi=90°$. The smallest losses are calculated in the case of specular-reflection geometry, i.e., $\theta=2\psi$ (~3–4 keV). These values agree basically with the experimental losses for small scattering angles and $\psi<2°$, as presented in Fig. 7. But the experiments show a clearly smaller difference between the axial and planar channelings compared to the calculations, especially for small scattering angles. The reason may be that the theoretical model does not account for the corrugated electronic surface, which causes on average a lower electron density in the surface channels. Theoretically, the higher energy losses are found in the case of very small scattering angles, which is clearly in contradiction to the experiment. Additionally, the experimental values ΔE^{expt} exceed ΔE^{theo} with increasing scattering angle up to a factor of 2 in the case of planar channeling, i.e., $\phi=80°$. Taking equal scattering angles, ΔE^{expt} is larger for $\theta_{out}>\psi$ than for $\psi\geqslant\theta_{out}$ with $\theta=\psi+\theta_{out}$ (Fig. 7). Therefore, we assume that on the outgoing projectile path the electronic projectile-step interaction contributes significantly to the energy loss by an additional amount ΔE^{step}. But since particles need to overcome the next upward step when leaving the interaction zone of the former step, they are only detectable under certain minimum outgoing scattering angles θ_{min} (see Fig. 8).

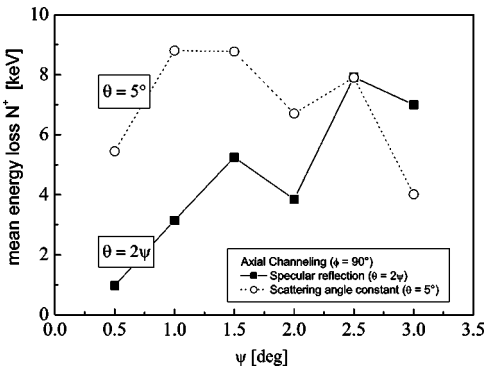

FIG. 7. Comparison of the experimental energy loss for 75 keV N^{5+} incoming and N^{+} outgoing ions depending on the angle of incidence ψ. Squares show losses in the case of specular-reflection scattering ($\theta=2\psi$), open circles in case of a fixed scattering angle of $\theta=5°$. Measurements are made along the [001]-surface channel.

To model the additional energy loss contribution coming from the step interaction, we evaluate θ_{min} assuming a parabolalike trajectory shape. As input we use step height z and terrace length x with $L_S=x+y$. The step height is given by

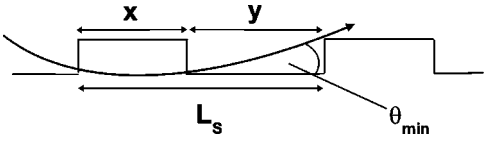

FIG. 8. Scheme of the step geometry and the definition of θ_{min} and L_S in the case of parabolalike particle trajectories. x gives the terrace length.

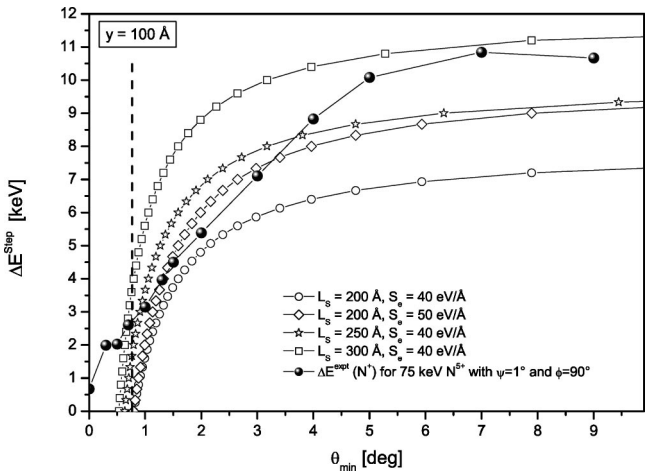

FIG. 9. Calculated inelastic energy losses for ions penetrating a surface step with length L_S and stopping power values S_e of 40 eV/Å and 50 eV/Å, respectively. The dashed-vertical line indicates the case that the projectile hits the step approximately at its turning point. For comparison, experimental energy losses for 75 keV N^{5+} and $\psi = 1°$ are given.

the crystalline plane distance to $z = a_0/2\sqrt{2}$ with $a_0 = 3.92$ Å as internuclear distance. We calculate the way the energy ΔE^{step} lost in a step interaction depends on θ_{min} for particles passing a surface step with terrace length x (Fig. 9). We vary the electronic stopping power value S_e and also the average total step length L_S. Good qualitative agreement is achieved for the θ dependency as well as for the absolute energy loss values by using reasonable values for L_S (200–300 Å) and S_e (40–50 eV/Å), making the model feasible. The stopping power values correspond to calculations performed with the TRIM 95 code [31] for N ions transmitted through amorphous bulk Pt and are roughly by a factor of 2 higher than expected for planar surface channeling [14]. Our model assumes that particles leaving the surface steps under very small angles are not detectable due to further interactions with the next surface steps kicking them off plane. However, these particles might undergo long trajectories leading to comparably high energy losses. Therefore, the plateaulike features in the energy dependency on the scattering angle seen in Figs. 4 and 9 can be understood as a step-caused trajectory selection depending on θ.

IV. CONCLUSION

In conclusion, the energy loss of N ions scattered off a stepped Pt surface is found to consist of three contributions, namely, the elastic transfer to the target atoms (very small), the electronic stopping during planar and axial surface channeling (3–7 keV), and the electronic stopping during projectile-step interaction (a few keV, Fig. 9). The results of the charge state measurements support the assumption of complete neutralization on the incoming projectile path. In the region of the turning point the projectile interacts with surface steps leading to additional energy losses. At the end of the trajectory, a step collision defines the outgoing angle and charge state of the projectile. The increase of the energy loss with increasing scattering angle can be explained by simple geometrical arguments, considering a step interaction basically described by the parameters L_S and θ_{min}. The step influence on the energy loss dependency on θ is relatively strong, since step length and trajectory length have comparable ranges. Our model shows good qualitative agreement with the experimental results and explains as well the enhanced energy loss as the enhanced N^{2+} yield percentage with higher scattering angles.

ACKNOWLEDGMENTS

We thank R. Morgenstern for many fruitful discussions. Financial support was provided by the Deutsche Forschungsgemeinschaft (DFG).

[1] D. Niemann, M. Grether, M. Rösler, and N. Stolterfoht, Phys. Rev. Lett. **80**, 3328 (1998).
[2] J. Limburg, S. Schippers, I. Hughes, R. Hoekstra, R. Morgenstern, S. Hustedt, N. Hatke, and W. Heiland, Phys. Rev. A **51**, 3873 (1995).
[3] J. Limburg, S. Schippers, R. Hoekstra, R. Morgenstern, H. Kurz, F. Aumayr, and H.-P. Winter, Phys. Rev. Lett. **75**, 217 (1995).
[4] T. Neidhart, F. Pichler, F. Aumayr, H.-P. Winter, M. Schmid, and P. Varga, Phys. Rev. Lett. **74**, 5280 (1995).
[5] M. Sporn, G. Libiseller, T. Neidhart, M. Schmid, F. Aumayr, H.-P. Winter, P. Varga, M. Grether, D. Niemann, and N. Stolterfoht, Phys. Rev. Lett. **79**, 945 (1997).
[6] K. Kuroki, T. Takahira, Y. Tsuruta, N. Okabayashi, T. Azuma, K. Komaki, and Y. Yamazaki, Phys. Scr. T **80**, 557 (1999).
[7] N. Stolterfoht, A. Arnau, M. Grether, R. Köhrbrück, A. Spieler, R. Page, A. Saal, J. Thomaschewski, and J. Bleck-Neuhaus, Phys. Rev. A **52**, 445 (1995).
[8] L. Folkerts, S. Schippers, D.M. Zehner, and F.W. Meyer, Phys. Rev. Lett. **74**, 2204 (1995); **75**, 983(E) (1995).
[9] F. Meyer, L. Folkerts, and S. Schippers, Nucl. Instrum. Methods Phys. Res. B **100**, 366 (1995).
[10] D. Niemann, M. Grether, A. Spieler, N. Stolterfoht, C. Lemell, F. Aumayr, and H.P. Winter, Phys. Rev. A **56**, 4774 (1997).
[11] R. Morgenstern, H. Khemliche, and R. Hoekstra, Appl. Phys. A: Mater. Sci. Process. **67**, 705 (1998).
[12] J. Thomaschewski, J. Bleck-Neuhaus, M. Grether, A. Spieler, and N. Stolterfoht, Phys. Rev. A **57**, 3665 (1998).
[13] H. Winter, C. Auth, R. Schuch, and E. Beebe, Phys. Rev. Lett. **71**, 1939 (1993).
[14] A. Robin, N. Hatke, A. Närmann, M. Grether, D. Plachke, J. Jensen, and W. Heiland, Nucl. Instrum. Methods Phys. Res. B **164-165**, 566 (2000).
[15] A. Robin, W. Heiland, J. Jensen, J.I. Juaristi, and A. Arnau, Phys. Rev. A **64**, 052901 (2001).
[16] W. Huang, H. Lebius, R. Schuch, M. Grether, and N. Stolterfoht, Phys. Rev. A **58**, 2962 (1998).
[17] A. Robin, J. Jensen, D. Ostermann, and W. Heiland, Nucl.

Instrum. Methods Phys. Res. B **193**, 573 (2002).
[18] A. Niehof and W. Heiland, Nucl. Instrum. Methods Phys. Res. B **48**, 306 (1990).
[19] H.D. Betz, Rev. Mod. Phys. **44**, 465 (1972).
[20] S. Speller, J. Kuntze, T. Rauch, J. Bömermann, M. Huck, M. Aschoff, and W. Heiland, Surf. Sci. **366**, 251 (1996).
[21] A. Hoffknecht, Master's thesis, Universität Osnabrück, 1996.
[22] A. Arnau, F. Aumayr, P. Echenique, M. Grether, W. Heiland, J. Limburg, R. Morgenstern, P. Roncin, S. Schippers, and R. Schuch *et al.*, Surf. Sci. Rep. **27**, 113 (1997).
[23] J. Burgdörfer, P. Lerner, and F.W. Meyer, Phys. Rev. A **44**, 5674 (1991).
[24] R. Pfandzelter, Phys. Rev. B **57**, 15 496 (1998).
[25] C. Lemell, H.P. Winter, F. Aumayr, J. Burgdörfer, and F. Meyer, Phys. Rev. A **53**, 880 (1996).
[26] H. Khemliche, J. Limburg, R. Hoekstra, R. Morgenstern, N. Hatke, E. Luderer, and W. Heiland, Nucl. Instrum. Methods Phys. Res. B **125**, 116 (1997).
[27] L.C. Northcliffe, Annu. Rev. Nucl. Sci. **13**, 67 (1963).
[28] S. Schippers, *Die Wechselwirkung Hochgeladener Lonen mit Platin und Blei Einkristall-Oberfläschen* (Verlag Shaker, Aachen, 1993) (Ph.D. thesis, Universität Osnabrück, 1992).
[29] N. Hatke, A. Hoffknecht, S. Hustedt, J. Limburg, I. Hughes, R. Hoekstra, W. Heiland, and R. Morgenstern, Nucl. Instrum. Methods Phys. Res. B **115**, 165 (1996).
[30] M. Fritz, K. Kimura, H. Kuroda, and M. Mannami, Phys. Rev. A **54**, 3139 (1996).
[31] J.F. Ziegler, J.P. Biersack, and U. Littmark, *The Stopping and Range of Ions in Solids* (Pergamon Press, New York, 1985).
[32] P.M. Echenique, R.M. Nieminen, J.C. Ashley, and R.H. Ritchie, Phys. Rev. A **33**, 897 (1986).